Applied Catalysis B: Environmental 158–159 (2014) 209–216

Contents lists available at ScienceDirect

Applied Catalysis B: Environmental

journal homepage: www.elsevier.com/locate/apcatb

Carbon-supported PdSn and Pd_3Sn_2 anodes for glucose electrooxidation in alkaline media

A. Brouzgou [a], S. Song [b], P. Tsiakaras [a,*]

[a] Department of Mechanical Engineering, School of Engineering, University of Thessaly, Pedion Areos, 38334 Volos, Greece
[b] State Key Laboratory of Optoelectronic Materials and Technologies, The Key Lab of Low-carbon Chemistry & Energy Conservation of Guangdong Province, School of Physics and Engineering, Sun Yat-sen University, Guangzhou 510275, China

ARTICLE INFO

Article history:
Received 4 November 2013
Received in revised form 14 March 2014
Accepted 29 March 2014
Available online 5 April 2014

Keywords:
Glucose electrooxidation
Alkaline media
Pd_xSn_y/C electrocatalysts
Direct glucose fuel cells

ABSTRACT

PdSn (20 wt.%) and Pd_3Sn_2 (20 wt.%) nanoparticles supported on Vulcan XC-72 carbon powders are prepared by a modified microwave-assisted polyol method and studied for the reaction of glucose electrooxidation in alkaline media. The as-prepared electrocatalysts are characterized by X-Ray Diffraction (XRD), Transmission Electron Microscopy (TEM), Cyclic Voltammetry (CV) and Chronoamperometry (CA). For comparison reasons, Pd/C (20 wt%) is also prepared. According to the CV results, the electrochemical active surface areas (EASA) were in the following order: Pd_3Sn_2/C > PdSn/C > Pd/C (28.8, 22.8 and 10.3 $m^2\ g^{-1}$). It is found that for glucose electrooxidation, at room temperature Pd_3Sn_2/C exhibited the highest electrocatalytic activity, 3.64 mA cm^{-2}, which is increased up to 5.7 mA cm^{-2}, as the temperature increases to 40 °C. The effect of concentration of both electrolyte and glucose on the activity is also studied and it is observed that the increase of the amount of both electrolyte and glucose enhances the rate of glucose electrooxidation. Additionally, from the chronoamperometric results, the diffusion coefficients of glucose are calculated to be 7.9×10^{-5}, 3.9×10^{-5} and 4.2×10^{-5} $cm^2\ s^{-1}$ for Pd_3Sn_2/C, PdSn/C and Pd/C, respectively.

1. Introduction

Glucose has been attracting much interest due to its importance as fuel for Direct Glucose Fuel Cells (DGFCs) and their applications as implantable human devices [1–3] as well as due to its high energy density (4430 W h kg^{-1}). Its complete oxidation to carbon dioxide can produce 24 electrons through the following chemical equations:

Anode reaction:

$$C_6H_{12}O_6 + 24OH^- \rightarrow 6CO_2 + 18H_2O + 24e^- \quad (1)$$

Cathode reaction:

$$6O_2 + 12H_2O + 24e^- \rightarrow 24OH^- \quad (2)$$

Overall reaction:

$$C_6H_{12}O_6 + 6O_2 \rightarrow 6CO_2 + 6H_2O \quad (3)$$

However, further research is necessary since glucose is very stable and consequently hardly oxidized molecule. It is worth noting that to date glucose oxidation has gone through a process generating only two electrons [4], yielding mostly gluconic acid, according to the following chemical equations:

Anode reaction:

$$C_6H_{12}O_6 + 2OH^- \rightarrow C_6H_{12}O_7 + H_2O + 2e^- \quad (4)$$

Cathode reaction:

$$0.5O_2 + H_2O + 2e^- \rightarrow 2OH^- \quad (5)$$

Overall reaction:

$$C_6H_{12}O_6 + 0.5O_2 \rightarrow C_6H_{12}O_7 \quad (6)$$

According to literature, glucose-fed alkaline membrane fuel cells exhibit superior performance compared to proton conducting membrane fuel cells [5]. More precisely, when the electrolyte is changed from acidic to alkaline the kinetics of the glucose electrooxidation reaction (GER) and oxygen reduction reaction (ORR) in alkaline media is enhanced compared with those in acid media [6]. Moreover, in an anion exchanged membrane direct glucose fuel cell (AEM-DGFC) the electro-osmotic drag is directed from the cathode to the anode, which can reduce the fuel's crossover rate from the anode to cathode and thus improve fuel cell performance.

* Corresponding author. Tel.: +30 24210 74065; fax: +30 24210 74050.
E-mail addresses: tsiak@uth.gr, tsiak@mie.uth.gr (P. Tsiakaras).

http://dx.doi.org/10.1016/j.apcatb.2014.03.051
0926-3373/

In addition, the cost of AEMs is lower than that of PEMs (mostly Nafion®) [7,8].

Many attempts [9–14] have been made to develop efficient and stable electrocatalysts for glucose electro-oxidation mostly in alkaline media. Many of them have been focused on Pt [4,15] and Au [16,17] or on their bi-metallic catalysts, Pt–Bi [11], Pt–Pd [18], Pt–Ru [19], Pt–Au [9,20], Ag–Au [21–23] and tri-metallic catalysts [24], while Pd-based electrocatalysts [25–27] have not been studied extensively.

It has been proved [5,26], that in alkaline environment Pd-based electrocatalysts perform much better activity than Pt-based ones due to the quicker oxidation kinetics of various alcohols electrooxidation. Additionally, the use of palladium instead of platinum automatically reduces the cost of a fuel cell [28].

In acidic environment among the reported electrocatalysts, PtSn-based ones [29–31] have been proved to be most appropriate for ethanol electrooxidation which is also a hardly oxidized molecule. On the other hand, Pd-based electrocatalysts have received much research attention because of their higher activity in alcohol electrooxidation in alkaline media, compared to Pt-based ones [5].

Consequently based on the two above-mentioned facts and taking into consideration that glucose like ethanol [32] is a hardly oxidizable molecule, we consider that Pd-based electrocatalysts could be good candidates for glucose electrooxidation. In the present work, Pd_xSn_y/C electrocatalysts have been prepared, characterized and tested for the first time as future anodes for direct glucose fuel cells with the cyclic voltammetry and chronoamperometric techniques.

Physico-chemical characterization of the electrocatalysts was carried out using transmission electron microscopy (TEM) and X-ray diffraction (XRD). Their electrocatalytic activity towards glucose electrooxidation was examined by cyclic voltammetry (CV), while their stability and poisoning rate by chronoamperometric measurements. Moreover, the effects of temperature, concentration of glucose and electrolyte were also investigated.

2. Experimental

2.1. Electrocatalysts preparation

PdSn and Pd_3Sn_2 supported on Vulcan-XC 72 carbon electrocatalysts (the metal loading was 20 wt.% for all the catalysts) were prepared by a modified pulse-microwave assisted polyol synthesis procedure. In a beaker, the starting precursors ($PdCl_2$ and $SnCl_2$ provided by Strem Chemicals) were well mixed with ethylene glycol (EG) in an ultrasonic bath, and then XC-72 R carbon black (Cabot Corporation) was added into the above mixture. After the pH value of the system was adjusted to 13 by the drop-wise addition of 1.0 M NaOH/EG, a well-dispersed slurry was obtained with ultrasonic stirring for 60 min. Thereafter, the slurry was microwave-heated in the pulse form 10 s on/10 s off for several times. In order to promote the adsorption of the suspended metal nanoparticles onto the carbon support, hydrochloric acid was adopted as the sedimentation promoter and the solution was re-acidified with a pH value of about 2–4. The resulting black solid sample was filtered, washed and dried at 80 °C for 10 h in a vacuum oven [33]. For the sake of comparison 20 wt% Pd/C was similarly prepared, characterized and examined for glucose electrooxidation in alkaline media.

2.2. Physico-chemical characterization

XRD measurements were carried out with the aid of a D/Max-IIIA (Rigaku Co., Japan) employing Cu K_α ($\lambda = 0.15406$ nm) as the radiation source at 40 kV and 40 mA. Catalysts were investigated by TEM using a Philips CM12 microscope (resolution 0.2 nm), provided with high resolution camera, at an accelerating voltage of 120 kV. Suitable specimens for TEM analyses were prepared by ultrasonic dispersion in *i*-propylic alcohol adding a drop of the resultant suspension onto a holey carbon supported grid.

2.3. Electrochemical characterization

All the electrochemical measurements were conducted with AMEL 5000 electrochemical station in a three-electrode model cell 497 (AMEL) with a mercury/mercury oxide (Hg/HgO) (0.098 V *vs.* NHE) and platinum wire as the reference electrode and counter electrode, respectively. The thin catalyst film was prepared onto a glassy carbon disk surface with a diameter of 0.3 cm. A mixture containing 5.0 mg electrocatalyst, 1.8 mL ethanol and 0.2 mL Nafion solution (5 wt.%, Dupont Company) was ultrasonicated for 40 min to obtain a well-dispersed ink. The catalyst ink was then quantitatively (10 μL) transferred onto the surface of the glassy carbon electrode and dried under infrared lamp to obtain a catalyst thin film. The electrochemical tests were performed initially in 0.5 M KOH (Sigma Aldrich) aqueous solutions containing 0.5 M glucose

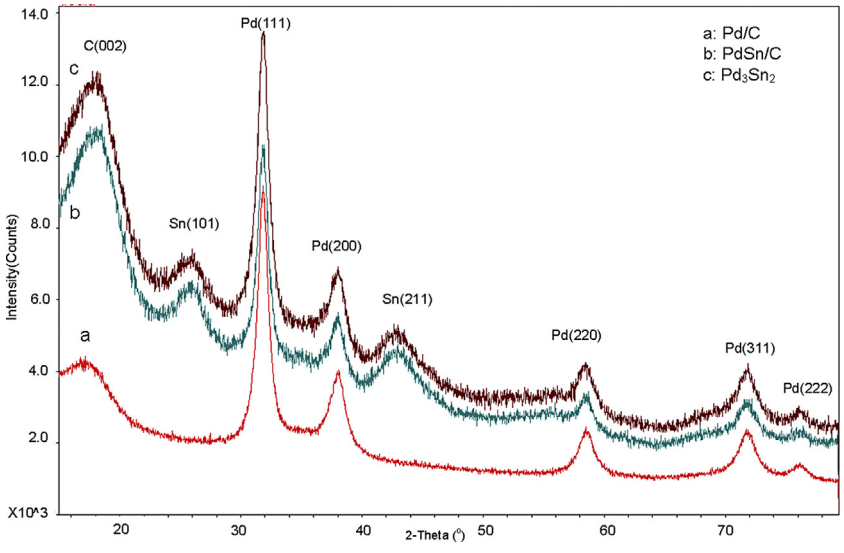

Fig. 1. XRD results of the as-prepared carbon supported Pd/C and Pd_xSn_y/C electrocatalysts.

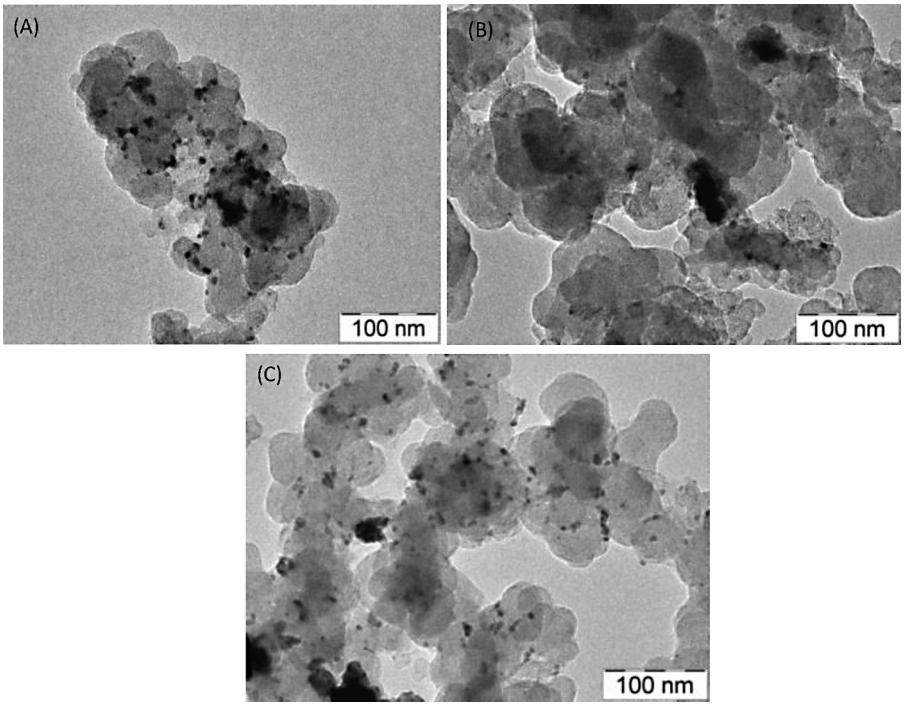

Fig. 2. TEM images of Pd_3Sn_2/C (A), PdSn/C (B) and Pd/C (C).

(Sigma Aldrich), for the electrochemical activity evaluations. Then the effect of the concentration of the electrolyte (0.1, 0.3, 0.5, 1 and 2 M KOH) for various glucose concentrations (0.02, 0.05, 0.2 and 0.5 M glucose) was investigated. Moreover, the effect of temperature (25–40 °C) on glucose electrooxidation was also investigated. Before each experiment, the solution was bubbled for 30 min with high-purity N_2 in order to remove the dissolved oxygen. Moreover, before each measurement, each catalyst was applied under continuous potential cycling until stable electrochemical signals were received. It should be noted that all the potentials are referred to Hg/HgO reference electrode without specification.

3. Results and discussion

3.1. Physico-chemical characterization

XRD patterns for the as-prepared electrocatalysts are shown in Fig. 1. For all three samples, the first peak at 25° is associated with the Vulcan XC-72 carbon. Then, there are five observed characteristic diffraction peaks at *ca.* 38°, 45°, 65°, 79° and 83° belonging to the face-centred cubic (fcc) phase of Pd (1 1 1), (2 0 0), (2 2 0), (3 1 1) and (2 2 2), respectively.

The (1 1 1) plane has the largest intensity among those planes, which becomes more intense as the palladium ratio is increased (Pd_3Sn_2/C). The two peaks that appear at *ca.* 33° and 50° are attributed to the Sn plane (1 0 1) and (2 1 1), respectively.

Table 1 lists the crystallites sizes and the corresponding lattice parameters calculated from the Pd (2 2 0) diffraction peak using the Scherrer formula and Bragg equations [34]. It can be clearly seen (Table 1) that the lattice parameter decreases in the order: PdSn/C = Pd/C > Pd_3Sn_2/C. As it is observed from the last two digits of lattice parameters values the one of Pd_3Sn_2/C electrocatalyst is a little higher.

Table 1
Structural parameters of the as-prepared catalysts.

Catalysts	Crystallite size (nm)	Nanoparticles size (nm)	Lattice parameter (nm)
Pd/C	8.2	~9.0	0.38645
PdSn/C	8.1	~8.0	0.38645
Pd_3Sn_2/C	7.8	~8.0	0.38636

Fig. 2 depicts the typical TEM micrographs for Pd/C, PdSn/C and Pd_3Sn_2/C, respectively. As it can be seen, Pd/C and Pd_3Sn_2/C have better dispersion than PdSn/C. For the binary catalysts, the metal particle size becomes smaller than that of the single metal, in agreement with the calculated values from XRD spectra.

3.2. Electrochemical characterization

The CV technique was used to determine the electrochemical active surface area and the catalytic activity of the examined electrocatalysts towards glucose electrooxidation. The currents (recorded in Figs. 3–9) have been normalized to the working

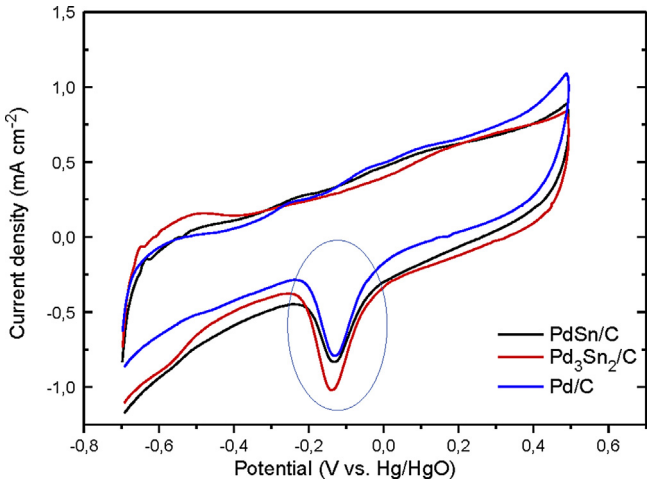

Fig. 3. Cyclic voltammograms for Pd/C, PdSn/C and Pd_3Sn_2/C in 0.5 M KOH at 25 °C, 20 mV s^{-1}.

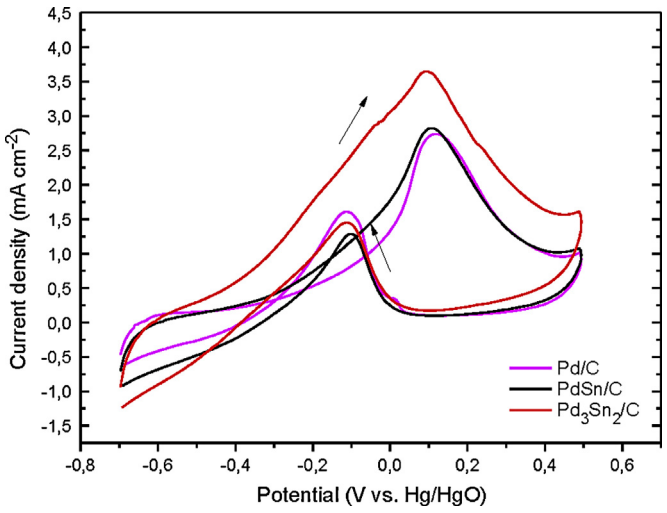

Fig. 4. Cyclic voltammograms for Pd/C, PdSn/C and Pd_3Sn_2/C in 0.5 M KOH + 0.5 M glucose at 25 °C, 20 mV s^{-1}.

electrode geometrical area ($A = 0.07\ cm^2$). It is well known that the catalytic activity of an electrode material depends upon its geometrical and electronic properties. As described elsewhere [35], the S_{ESA} of the electrodes have been measured by determining the coulombic charge (Q) for the reduction of palladium oxide (as indicated from the ellipse in Fig. 3) of CV measurements in 0.5 M KOH, at 25 °C for 20 mV s^{-1} scan rate (Fig. 3). The CV cycles depicted in Fig. 3 are those after multiple potential cycling until a stable shape of the curves was obtained. Calculated values of the S_{ESA}, as shown in Table 2, are estimated using the following equation:

$$S_{ESA} = \frac{Q \quad (\mu C\ \ cm^{-2})}{\{Q_{PdO} \quad (\mu C\ \ cm^{-2}_{Pd})\ Pd_{loading} \quad (mg\ \ cm^{-2}) \times 10\}} \tag{7}$$

where $Q_{PdO} = 405\ \mu C\ cm^{-2}$ is the charge value for the reduction of PdO monolayer [36] and Q is the experimental charge for the reduction of palladium oxide.

As can be clearly seen from the CV curves shown in Fig. 3, Pd_3Sn_2/C shows higher peak current density of PdO reduction in the potential range between −0.2 and 0 V than the other electrocatalysts. This demonstrates that Pd_3Sn_2/C has a higher electrochemical active surface area, compared to Pd/C, and PdSn/C, as it is also reported in Table 1, 28.8 $m^2\ g^{-1}$ for Pd3Sn2/C, 10.3 $m^2\ g^{-1}$ for Pd/C, and 22.8 $m^2\ g^{-1}$ for PdSn/C, respectively.

Pd-utilization effectiveness factor (=100 × observed EASA, $m^2\ g^{-1}$/448 $m^2\ g^{-1}$) was also estimated considering the surface area for 100% utilization of 1 g Pd as ~448 m^2 (=the required charge to reduce 1 g Pd^{+2} is 1813.3 C/405 μC cm^{-2}) [37] and reported in Table 2. Pd utilization is the highest for the Pd_3Sn_2 (6.4%).

In Fig. 3, a typical electrochemical behaviour of Pd-based electrocatalysts in alkaline media can be observed. The first peak from −0.6 to −0.4 V can be attributed to the oxidation of the adsorbed and absorbed hydrogen [38–40]. The peak that appears from −0.3 to −0.1 V is attributed to the formation of $PdOH^-$, which partially overlaps the hydrogen desorption peak, while the third peak which starts from −0.1 to 0.3 V can be attributed to the formation of the palladium(II) oxide layer on the surface of the catalyst. In general, the mechanism of glucose oxidation process on Pd-based electrocatalysts remains unclear. However, it has been widely accepted that OH^- ions are firstly chemisorbed in the initial stage of the oxide formation, and then at higher potentials they are transformed into higher valence oxides through Eqs. (8)–(11) [40–42]:

$$Pd - H_{abs/ads} + OH^- \rightarrow Pd + H_2O + e^- \tag{8}$$

$$Pd + OH^- \rightleftarrows Pd - OH_{ads} + e^- \tag{9}$$

$$Pd - OH_{ads} + OH^- \rightleftarrows Pd - O + H_2O + e^- \tag{10}$$

$$Pd - OH_{ads} + Pd - OH_{ads} \rightleftarrows Pd - O + H_2O \tag{11}$$

During the backward scan the reduction of the Pd(II) oxides (according to Eq. (12)) is responsible for the negative peak at ~−0.15 V [40,41]:

$$Pd - O + H_2O + 2e^- \rightleftarrows Pd + 2OH^- \tag{12}$$

3.3. Glucose electrooxidation reaction (GOR)

The CV results for the GOR, depicted in Fig. 4, clearly indicate that Pd_3Sn_2/C exhibits the highest electrocatalytic activity. Its enhanced activity (compared with Pd/C and PdSn/C) could be mainly attributed to the Sn content [43] and then to its synergistic effect, considering the very small difference in their lattice parameter and their close crystallite size values (Table 1). However, when the Sn content is more than 43 at.%, the catalytic efficiency is reduced.

According to Fig. 4, during the forward potential scanning, the formation of palladium oxides (PdO) at ~0.1 V and glucose electrosorption to form an adsorbed intermediate takes place.

Moreover, compared with the results in Fig. 3, it can be known that the hydrogen desorption/sorption region (<−0.45 V) is suppressed in the presence of glucose in the solution. The observed decrease of current density at more positive potentials than the peak potential value could be due to the formation of thick palladium oxide films which competes for surface adsorption sites with glucose and in turn inhibits the electrooxidation of glucose [44]. In the backward scanning the peak that appeares at ~−0.1 V, is attributed to the direct glucose oxidation again, since the formed PdO during the forward scan has been reduced to Pd [45]. From Fig. 4 it can be seen that in the case of Pd/C, the backward oxidation peak of the oxides is higher compared to the other two electrocatalysts (see Table 3), indicating that Pd/C electrocatalyst is a little more tolerant to poisonous intermediates.

Furthermore, the onset potential for the Pd_3Sn_2/C (−0.56 V) is more negative compared to that of Pd/C (−0.32 V) and of PdSn/C (−0.38 V).

Recently, we have presented in literature [46] our investigation regarding the reaction of glucose electrooxidation on Pd_xRh_y/C. Comparing the electrocatalytic activity of Pd_xRh_y/C with that of Pd_3Sn_2/C presented in the present work, it can be deduced that the latter exhibits relatively higher current density values.

Table 2
Electrocatalytic kinetic parameters on different electrodes in 0.5 M KOH, at 25 °C, 20 mV s^{-1}.

Catalysts	Pd loading (μg cm^{-2})	EASA ($m^2\ g^{-1}$)	Pd utilization (%)
Pd/C	72.0	10.3	2.3
PdSn/C	34.0	22.8	5.0
Pd_3Sn_2/C	41.0	28.8	6.4

Table 3
Cyclic voltammetry parameters on different electrodes in 0.5 M KOH + 0.5 glucose, at 25 °C, 20 mV s^{-1}.

Catalyst	Forward scan j_p/mA cm^{-2} E_p/mV	Backward scan j_p/mA cm^{-2} E_p/mV
Pd/C	2.70 0.11	1.60 -0.10
PdSn/C	2.80 0.10	1.40 -0.11
Pd_3Sn_2/C	3.70 0.08	1.23 -0.09

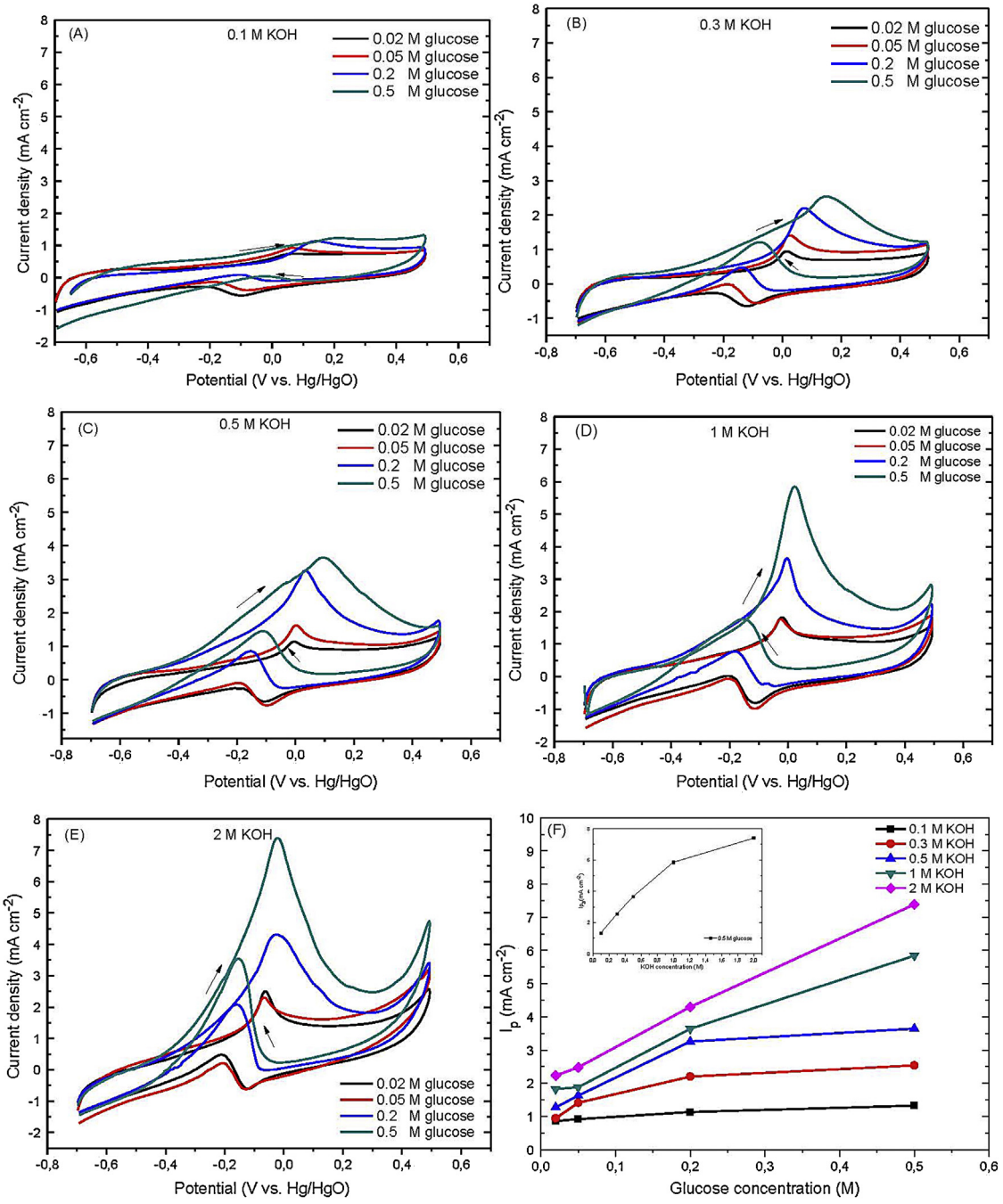

Fig. 5. Cyclic voltammograms of the Pd_3Sn_2/C electrocatalyst in: (A) 0.1, (B) 0.3, (C) 0.5, (D) 1 and (E) 2 M KOH containing *y* (=0.02, 0.05, 0.2, and 0.5M) glucose (scan rate: 20mVs^{-1}, room temperature). (F) Peak current density dependence of glucose concentration. The inset of (F) shows the OH^- concentration effect, at 0.5M glucose.

3.4. *Effect of glucose's and electrolyte's concentration*

The cyclic voltammograms of the Pd_3Sn_2/C electrocatalyst, which exhibits the highest activity towards glucose electrooxidation, for different glucose and electrolyte concentrations are depicted in Fig. 5. As it can be distinguished, the oxidation current increases as the concentrations of glucose and of potassium hydroxide (electrolyte) increase. Moreover, with electrolyte concentration increasing, the peak potential shifts to more negative values, suggesting that the KOH concentration has a favourable effect on glucose oxidation [47]. The increase of KOH concentration may lead to a greater coverage of the reactive $Pd–OH_{ads}$, which may facilitate glucose oxidation. A linear relationship is observed between glucose concentration and peak current density (Fig. 5(F)) in the case of high electrolyte concentration values (1 M and 2 M KOH).

Tafel plots were obtained from the onset region of the polarization curves [48] from the limited form of the Butler–Volmer equation:

$$\log\ i = \log\ i_o + \left(\frac{\alpha_a nF}{2.303RT}\right)\eta \qquad (13)$$

where η is the overpotential, i_o is the exchange current density and α_a is the anodic transfer coefficient, n (=1) is the number of electrons that take part in the redox process, F is the Faraday constant, R is the universal gas constant and T is the temperature in K. The Tafel

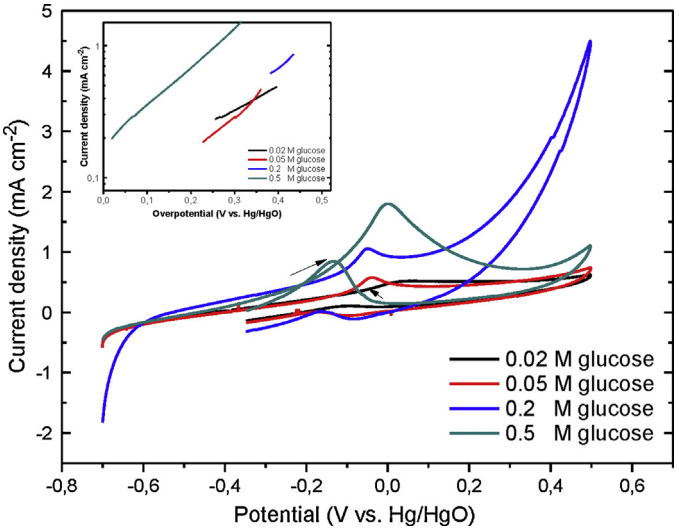

Fig. 6. Cyclic voltammograms of Pd_3Sn_2/C electrocatalyst in 0.5 mol L^{-1} KOH containing (=0.02, 0.05, 0.2, and 0.5 mol L^{-1}) glucose (scan rate: 5 mV s^{-1}, room temperature); inset: The respective Tafel plots.

equation has been applied to the kinetically controlled CV's curve region (from the onset to the peak potential).

As it is observed from Fig. 6, with increasing glucose concentration, the catalytic activity is enhanced. In contrast to the obtained CV curves (for 0.02, 0.05 and 0.5 M glucose) in case of 0.2 M glucose, when the anodic sweep turns to cathodic sweep (at 0.5 V) an augmentation of the curve is observed. This behaviour was also observed in our previous study [46] for 0.2 M glucose. According to Becerik et al. [45] the observed extended curve at more positive potentials means the oxidation of some of the intermediates that have been formed at lower potentials (<0.5 V) takes place, restoring some active sites. On the other hand the depression of the 0.02, 0.05 and 0.5 M glucose CV curves at 0.5 V potential means the blockage of some active sites.

From Fig. 6, the exchange current density and the transfer coefficient are calculated. The respective values are given in Table 4. The exchange current density values are 0.090, 0.042, 0.056 and 0.190 mA cm^{-2} as well as 0.10, 0.165, 0.16 and 0.17 charge

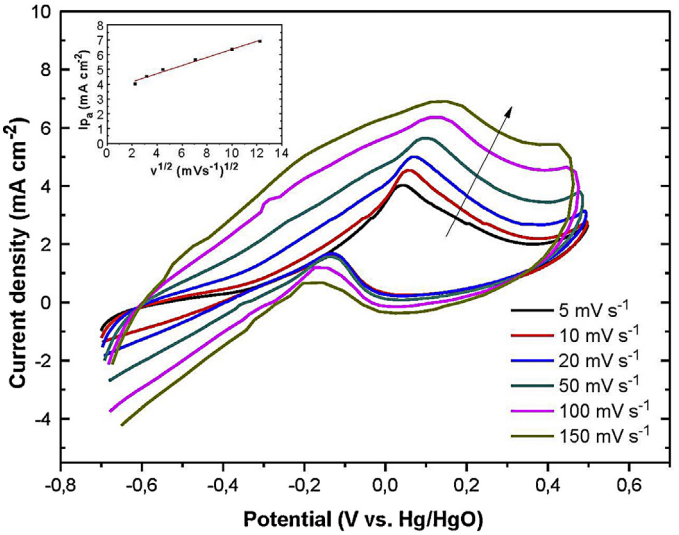

Fig. 7. Cyclic voltammograms of the Pd_3Sn_2/C electrocatalyst in 0.5 M KOH containing 0.5 M glucose at different scan rates in room temperature, inset: dependence of anodic peak current during the forward sweep on the square roots of potential sweep rate.

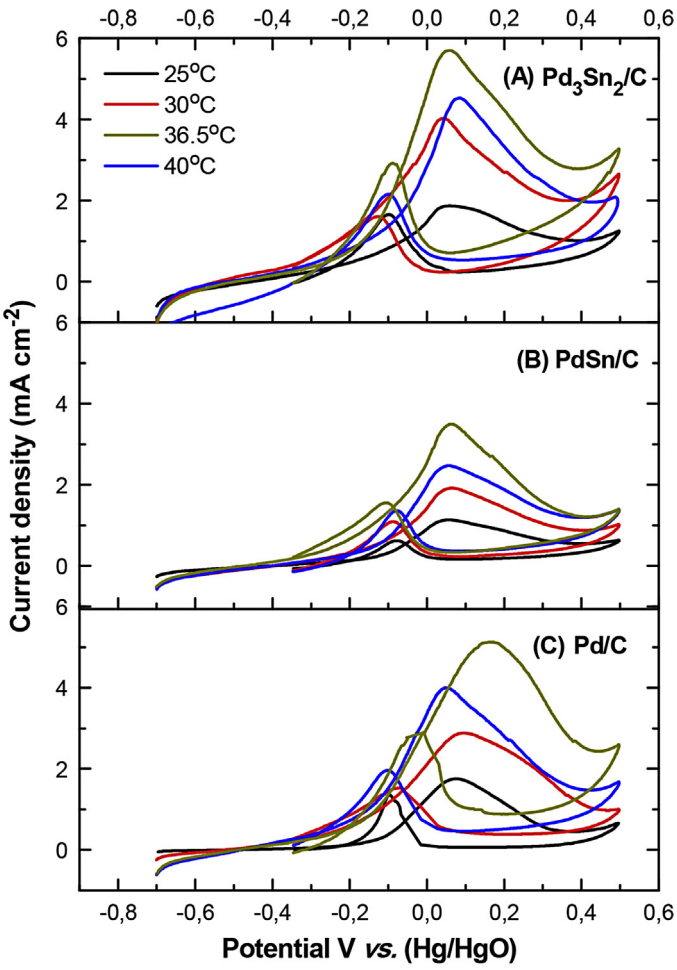

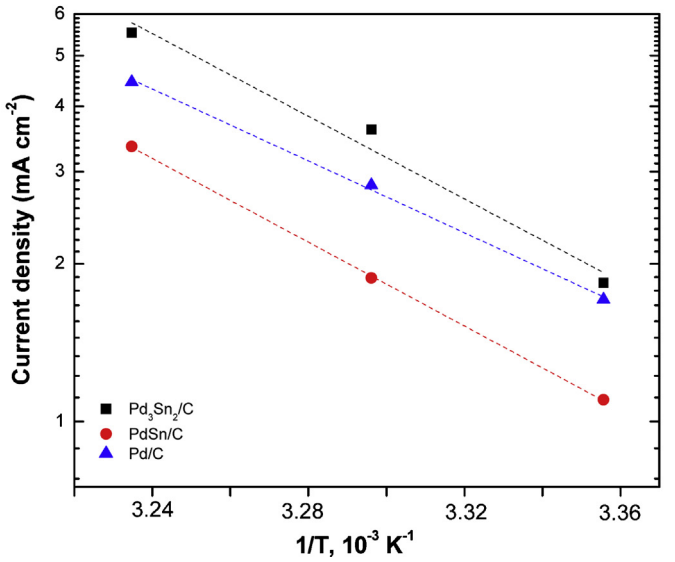

Fig. 8. Cyclic voltammograms at different temperature values (T = 25, 30, 36.5 and 40 °C), in 0.5 mol L^{-1} KOH containing 0.5 mol L^{-1} glucose, 5 mV s^{-1} of: Pd_3Sn_2/C (A), PdSn/C (B) and Pd/C (C). (D) Arrhenius plots derived from (A–C).

transfer coefficients for 0.02, 0.05, 0.2 and 0.5 M glucose, respectively. The reversible potential values for 0.02, 0.05, 0.2 and 0.5 M glucose used for calculating Tafel parameters are −0.39, −0.43, −0.51 and −0.35 V, respectively. The calculated charge transfer values comparable with others from literature [49] are lower, and the exchange current density remains at relatively low values

Table 4
Kinetic parameters extracted from Tafel equation, of the Pd_3Sn_2/C catalyst in 0.5 M KOH for different glucose concentration values.

Glucose concentration	Exchange current density (mA cm^{-2})	Charge transfer coefficient
0.02	0.090	0.10
0.05	0.042	0.165
0.2	0.056	0.16
0.5	0.190	0.17

indicating that further research is necessary for glucose electrooxidation reaction.

3.5. Effect of the scan rate

The kinetics of glucose oxidation reaction was further investigated. Fig. 7 depicts the CVs of the Pd_3Sn_2/C in 0.5 M glucose + 0.5 M KOH solution. The scan rate was increased from 5 to 150 mV s^{-1}.

The anodic peak current density (positive scan) is linearly proportional to the square root (the inset of Fig. 7) of the scan rate (R^2 = 0.98), indicating that the electrode process is controlled *via* diffusion [50]. This statement agrees with Becerik and Kadirgan [45] who also found that glucose electrooxidation on single palladium electrocatalyst was diffusion limited. According to Stasiukaitis et al. [51] and Zuo et al. [52] the fact that the straight line (I_p *vs* $v^{1/2}$) does not cross the zero point is attributed to the small working electrode radius.

Along with the scan rate increasing, glucose electrooxidation reaction is enhanced; however, peak potential shifts to higher values. The shift of the peak potential to higher values is possibly due to the IR drop generated at higher current density values [53].

3.6. Effect of temperature

The effect of temperature on glucose electrooxidation reaction was also examined for T = 30, 36.5 and 40 °C. It has been proved [54] that glucose rapidly degrades above 40 °C as evidenced by the rapid change of the colour to yellow-brown and a caramel-like smell. This is the reason that the maximum examined temperature in the present work was also limited to 40 °C. As is observed in Fig. 8, with the increase in the temperature value, the current density increases, while the peak potential shifts to more positive values.

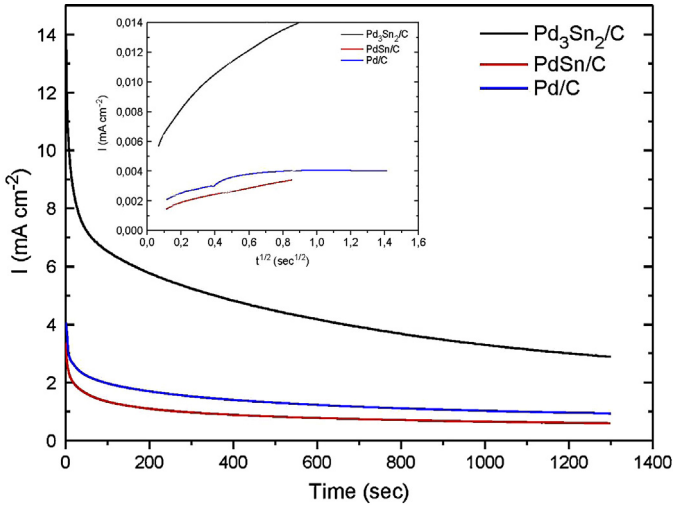

Fig. 9. Chronoamperometric curves at −0.13 V (*vs.* Hg/HgO) for 1300 s, in a 0.5 mol L^{-1} KOH with 0.5 mol L^{-1} glucose solution, Inset: Cottrell plot.

The apparent activation energy E_a can be calculated from the current density values measured at different temperatures using the following equation:

$$E_a = R\left(\frac{d(\ln\ I)}{d\left(1/T\right)}\right) \quad (14)$$

In Fig. 8(D), the Arrhenius plots, extracted from Fig. 8(A–C), are depicted. The apparent activation energy values, at 0.075 V (*vs.* Hg/HgO), are calculated to be 75.6 kJ mol^{-1}(18 kcal mol^{-1}), 76.5 kJ mol^{-1}), (18.3 kcal mol^{-1}) and 65.7 kJ mol^{-1} (15.7 kcal mol^{-1}), for the Pd_3Sn_2/C, PdSn/C and Pd/C electrocatalysts, respectively. Becerik et al. [45] also studied glucose electrooxidation on Pd/C (0.1 M NaOH), calculating 10 kcal mol^{-1} for glucose electrooxidation.

3.7. Chronoamperometric measurements

Fig. 9 shows the chronoamperometric results for the examined electrocatalysts in 0.5 M KOH + 0.5 M glucose at 25 °C for 1300 s at a fixed potential (−0.13 V). An initial rapid decrease in the current density with time is observed for all catalysts. As it can be observed, this decay is higher for PdSn/C and Pd/C electrocatalysts than for Pd_3Sn_2/C; however, the current density of the last catalyst catches plateau over 2 mA cm^{-2} than that of Pd/C. From Fig. 9 the poisoning rate (δ) can be calculated by measuring the linear decay of the current for a period of more than 500 s using the following equation:

$$\delta = \left(\frac{100}{I_o}\right)\left(\frac{dI}{dt}\right)_{t>500\ s} \quad (15)$$

where $(dI/dt)_{t>500\ s}$ represents the slope of the linear portion of current decay and I_o the current at the beginning of polarization, back extrapolated from the linear current decay.

The poisoning rate was calculated to be 0.014, 0.008 and 0.002% s^{-1} for Pd_3Sn_2/C, PdSn/C and Pd/C, respectively. The poisoning rate is found to be more intense for the Pd_3Sn_2/C.

Moreover, chronoamperometry was employed for the investigation of glucose diffusion coefficient. Under the diffusion controlled regime conditions and according to the Cottrell equation [55] the current intensity is given by

$$I = \frac{nFAD^{1/2}C}{\pi^{1/2}t^{1/2}} \quad (16)$$

where A represents the geometric surface area of the disk electrode (0.07 cm^2), D the diffusion coefficient (cm^2 s^{-1}), C the bulk concentration of glucose (M), and F the Faraday's constant (96,485 C mol^{-1}). The slope of the linear plot of I *vs.* $t^{-1/2}$ can be used for the estimation of glucose diffusion coefficient. The calculated glucose diffusion coefficients are: 7.9×10^{-5}, 3.9×10^{-5} and 4.2×10^{-5} cm^2 s^{-1}, for Pd_3Sn_2/C, PdSn/C and Pd/C, respectively. The calculated values are reasonable according to that reported in literature [56].

4. Conclusions

Pd_xSn_y/C binary catalysts were synthesized by a modified pulse microwave assisted polyol method and were investigated for the reaction of glucose electrooxidation. The results were compared with Pd/C which was synthesized by the same method. The optimum Pd_3Sn_2/C exhibited the desirable activity for glucose electrooxidation, but according to chronoamperometric results it was poisoned faster when compared to the PdSn/C and Pd/C electrocatalysts. Moreover, from the chronoamperometric results glucose diffusion coefficient calculated for Pd_3Sn_2/C was 7.9×10^{-5} cm^2 s^{-1}, in agreement with that reported in literature.

Glucose electrooxidation reaction on Pd_3Sn_2/C was also studied for a range of values of temperature, glucose and electrolyte concentration. According to the cyclic voltammetric results, as temperature increases from 25 °C to 40 °C, the current density increases from 1.87 to 5.7 mA cm^{-2}. Additionally, at a constant glucose concentration, increasing electrolyte concentration from 0.1 to 2 M KOH, current density increases from 1.3 to 7.4 mA cm^{-2}. Increment of the current density is also observed when glucose concentration increases from 0.02 to 0.5 M, for all KOH concentrations. The observed increment becomes more intense at high (1 M and 2 M KOH) electrolyte concentration. Finally, studying the effect of scan rate indicates that the electrode process is diffusion limited.

Acknowledgements

A. Brouzgou is grateful to the European Union (European Social Fund—ESF) and Greek national funds through the Operational Program "Education and Lifelong Learning" of the National Strategic Reference Framework (NSRF)—Research Funding Program: Heracleitus II. Investing in knowledge society through the European Social Fund. The authors are also grateful to Dr. Frusteri Francesco of the CNR-TAE Institute for the TEM analysis.

References

[1] S. Calabrese Barton, J. Gallaway, P. Atanassov, Chem. Rev. 104 (2004) 4867–4886.
[2] H. Liu, B.E. Logan, Environ. Sci. Technol. 38 (2004) 4040–4046.
[3] M. Guerra-Balcázar, D. Morales-Acosta, F. Castaneda, J. Ledesma-García, L.G. Arriaga, Electrochem. Commun. 12 (2010) 864–867.
[4] N. Fujiwara, S.-i. Yamazaki, Z. Siroma, T. Ioroi, H. Senoh, K. Yasuda, Electrochem. Commun. 11 (2009) 390–392.
[5] A. Brouzgou, A. Podias, P. Tsiakaras, J. Appl. Electrochem. 43 (2013) 119–136.
[6] H.F. Cui, J.S. Ye, X. Lui, W.D. Zhang, F.S. Sheu, Nanotechnology 17 (2006) 2334–2339.
[7] L. An, T.S. Zhao, S.Y. Shen, Q.X. Wu, R. Chen, Int. J. Hydrogen Energy 35 (2010) 4329–4335.
[8] Y.S. Li, T.S. Zhao, W.W. Yang, Int. J. Hydrogen Energy 35 (2010) 5656–5665.
[9] X. Yan, X. Ge, S. Cui, Nanoscale Res. Lett. 6 (2011) 313.
[10] F. Xie, Z. Huang, C. Chen, Q. Xie, Y. Huang, C. Qin, Y. Liu, Z. Su, S. Yao, Electrochem. Commun. 18 (2012) 108–111.
[11] D. Basu, S. Basu, Electrochim. Acta 56 (2011) 6106–6113.
[12] L. An, T.S. Zhao, S.Y. Shen, Q.X. Wu, R. Chen, J. Power Sources 196 (2011) 186–190.
[13] M. Guerra-Balcázar, F.M. Cuevas-Muñiz, L. Álvarez-Contreras, L.G. Arriaga, J. Ledesma-García, J. Power Sources 197 (2012) 121–124.
[14] L. Li, K. Scott, E.H. Yu, J. Power Sources 221 (2013) 1–5.
[15] Q. Shen, L. Jiang, H. Zhang, Q. Min, W. Hou, J.-J. Zhu, J. Phys. Chem. C 112 (2008) 16385–16392.
[16] W. Huang, M. Wang, J. Zheng, Z. Li, J. Phys. Chem. C 113 (2009) 1800–1805.
[17] H. Yin, C. Zhou, C. Xu, P. Liu, X. Xu, Y. Ding, J. Phys. Chem. C 112 (2008) 9673–9678.
[18] J.P. Spets, Y. Kiros, M.A. Kuosa, J. Rantanen, M.J. Lampinen, K. Saari, Electrochim. Acta 55 (2010) 7706–7709.
[19] D. Basu, S. Basu, Electrochim. Acta 55 (2010) 5775–5779.
[20] D. Basu, S. Basu, Int. J. Hydrogen Energy 36 (2011) 14923–14929.
[21] Z. Liu, L. Huang, L. Zhang, H. Ma, Y. Ding, Electrochim. Acta 54 (2009) 7286–7293.
[22] C. Jin, I. Taniguchi, Mater. Lett.V 61 (2007) 2365–2367.
[23] F.M. Cuevas-Muñiz, M. Guerra-Balcázar, F. Castaneda, J. Ledesma-García, L.G. Arriaga, J. Power Sources 196 (2011) 5853–5857.
[24] D. Basu, S. Basu, Int. J. Hydrogen Energy 37 (2012) 4678–4684.
[25] Q. Wang, X. Cui, J. Chen, X. Zheng, C. Liu, T. Xue, H. Wang, Z. Jin, L. Qiao, W. Zheng, RSC Adv. 2 (2012) 6245–6249.
[26] Y. Kuang, B. Wu, D. Hu, X. Zhang, J. Chen, J. Solid State Electrochem. 16 (2012) 759–766.
[27] L.-M. Lu, H.-B. Li, F. Qu, X.-B. Zhang, G.-L. Shen, R.-Q. Yu, Biosens. Bioelectron. 26 (2011) 3500–3504.
[28] A. Brouzgou, S.Q. Song, P. Tsiakaras, Appl. Catal., B: Environ. 127 (2012) 371–388.
[29] W.J. Zhou, S.Q. Song, W.Z. Li, Z.H. Zhou, G.Q. Sun, Q. Xin, S. Douvartzides, P. Tsiakaras, J. Power Sources 140 (2005) 50–58.
[30] Y. Wang, S. Song, G. Andreadis, H. Liu, P. Tsiakaras, J. Power Sources 196 (2011) 4980–4986.
[31] A. Kowal, M. Li, M. Shao, K. Sasaki, M.B. Vukmirovic, J. Zhang, N.S. Marinkovic, P. Liu, A.I. Frenkel, R.R. Adzic, Nat. Mater. 8 (2009) 325–330.
[32] P.E. Tsiakaras, J. Power Sources 171 (2007) 107–112.
[33] S. Song, J. Liu, J. Shi, H. Liu, V. Maragou, Y. Wang, P. Tsiakaras, Appl. Catal., B: Environ. 103 (2011) 287–293.
[34] A. Pozio, M. De Francesco, A. Cemmi, F. Cardellini, L. Giorgi, J. Power Sources 105 (2002) 13–19.
[35] R. Pattabiraman, Appl. Catal., A: Gen. 153 (1997) 9–20.
[36] M.H. Seo, S.M. Choi, H.J. Kim, W.B. Kim, Electrochem. Commun. 13 (2011) 182–185.
[37] R.N. Singh, A. Singh, Anindita, Int. J. Hydrogen Energy 34 (2009) 2052–2057.
[38] T. Takamura, K.i. Minamiyama, J. Electrochem. Soc. 112 (1965) 333–335.
[39] J. Prabhuram, R. Manoharan, H.N. Vasan, J. Appl. Electrochem. 28 (1998) 935–941.
[40] M. Grdeń, A. Czerwiński, J. Solid State Electrochem. 12 (2008) 375–385.
[41] M.C. Jeong, C.H. Pyun, I.H. Yeo, J. Electrochem. Soc. 140 (1993) 1986–1989.
[42] L. Vračar, S. Burojević, N. Krstajić, Int. J. Hydrogen Energy 23 (1998) 1157–1164.
[43] M. Shao, Electrocatalysis in Fuel Cells: A non- and Low-Platinum Approach, Minhua Shao, London, 2013.
[44] L. Meng, J. Jin, G. Yang, T. Lu, H. Zhang, C. Cai, Anal. Chem. 81 (2009) 7271–7280.
[45] I. Becerik, F. Kadirgan, Electrochim. Acta 37 (1992) 2651–2657.
[46] A. Brouzgou, L.L. Yan, S.Q. Song, P. Tsiakaras, Appl. Catal., B: Environ. 147 (2013) 481–489.
[47] Z.X. Liang, T.S. Zhao, J.B. Xu, L.D. Zhu, Electrochim. Acta 54 (2009) 2203–2208.
[48] B.K. Boggs, G.G. Botte, Electrochim. Acta 55 (2010) 5287–5293.
[49] Q. Yi, W. Yu, Microchim. Acta 165 (2009) 381–386.
[50] J. Heinze, Angew. Chem. Int. Ed. 23 (1984) 831–847.
[51] P.V. Stasiukaitis, V. Skominas, J. Electroanal. Chem. 459 (1998) 121–133.
[52] X. Zuo, C. Xu, H. Xin, Electrochim. Acta 42 (1997) 2555–2558.
[53] M.A. Abdel Rahim, R.M. Abdel Hameed, M.W. Khalil, J. Power Sources 134 (2004) 160–169.
[54] L.H.E. Yei, B. Beden, C. Lamy, J. Electroanal. Chem. 246 (1988) 349–362.
[55] I. Danaee, M. Jafarian, F. Forouzandeh, F. Gobal, M.G. Mahjani, Int. J. Hydrogen Energy 33 (2008) 4367–4376.
[56] R.G. Mortimer, Physical Chemistry, 3rd edition, Elsevier Inc, Canada, 2008.